POLITECNICO
MILANO 1863

DIPARTIMENTO DI MECCANICA

mecc

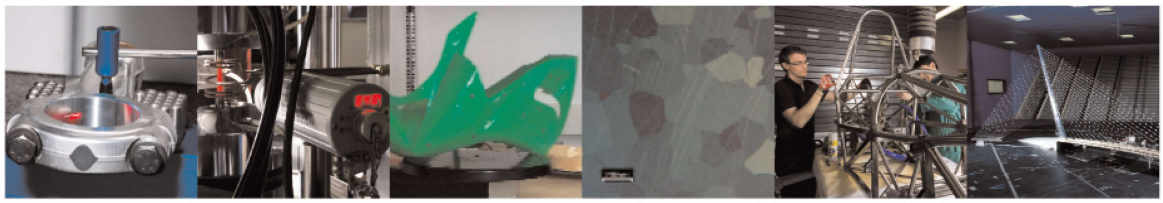

Selective laser melting of NiTi stents with open-cell and variable diameter

Simone Maffia, Valentina Finazzi, Francesca Berti, Francesco Migliavacca, Lorenza Petrini, Barbara Previtali, Ali Gökhan Demir

This is a post-peer-review, pre-copyedit version of an article published in Smart Materials and Structures. The final authenticated version is available online at:
http://dx.doi.org/10.1088/1361-665X/ac1908

Selective laser melting of NiTi stents with open-cell and variable diameter

Simone Maffia[a], Valentina Finazzi[a,b], Francesca Berti[c],

Francesco Migliavacca[c], Lorenza Petrini[b], Barbara Previtali[a], Ali Gökhan Demir[a,*]

[a]*Department of Mechanical Engineering, Politecnico di Milano, Via La Masa 1, 20156 Milan, Italy*
[b]*Department of Civil and Environmental Engineering, Politecnico di Milano, Piazza Leonardo da Vinci 32, 20133 Milan, Italy*
[c]*Laboratory of Biological Structure Mechanics, Department of Chemistry, Materials and Chemical Engineering 'Giulio Natta', Politecnico di Milano, Piazza Leonardo da Vinci 32, 20133 Milan, Italy*

*Corresponding author: aligokhan.demir@polimi.it

Selective laser melting of NiTi stents with open-cell and variable diameter

Simone Maffia[a], Valentina Finazzi[a,b], Francesca Berti[c], Francesco Migliavacca[c], Lorenza Petrini[b], Barbara Previtali[a], Ali Gökhan Demir[a,*]

[a]*Department of Mechanical Engineering, Politecnico di Milano, Via La Masa 1, 20156 Milan, Italy*
[b]*Department of Civil and Environmental Engineering, Politecnico di Milano, Piazza Leonardo da Vinci 32, 20133 Milan, Italy*
[c]*Laboratory of Biological Structure Mechanics, Department of Chemistry, Materials and Chemical Engineering 'Giulio Natta', Politecnico di Milano, Piazza Leonardo da Vinci 32, 20133 Milan, Italy*
*Corresponding author: aligokhan.demir@polimi.it

Abstract

This work investigates the processing of NiTi open-cells peripheral stents with variable diameter by SLM and consecutive heat treatments. The production of open-cell designs via SLM requires dedicated processing strategies to avoid the use of support structures with comparable dimensions to the stent struts. Process parameters were studied with an SLM system operating with pulsed wave emission to assess the geometrical fidelity and the density of thin struts. The novel stent mesh was designed and produced employing gaps with un-melted powder between the consecutive cells along the build direction. Solution annealing and stress relieving treatments were assessed after SLM. The results show that regular struts with high density (>99.5%) with an austenitic transformation finish below the room temperature can be achieved with SLM and dedicated heat treatment.

Keywords: Nitinol stent; patient-specific design; additive manufacturing.

1. Introduction

Peripheral artery disease (PAD), namely the pathological reduction of the arterial lumen of lower limb vessels, affects 12% of the world's adult population [1]. The clinical gold standard for PAD treatment of is represented by endovascular stenting. This procedure is performed through mini-invasive catheters that allow to introduce into the body metallic nets, named stents: once reached the stenotic portion of the vessel, the stent opening allow to recover the original blood flow and provide sufficient radial force during the vessel's healing [2]. Peripheral stents are made of Nickel-Titanium (NiTi) alloy: they exploit superelasticity at body temperature to withstand the considerable deformations induced n the stent struts due to minimally invasive implantation and, successively,

during leg movements [3–5]. The NiTi stents are conventionally laser cut from tubular precursors [6]. Consequently they are chemically etched and/or electrochemically polished to remove the dross generated during the laser cutting operation. They are then expanded to the desired size in a die and shape setting is applied. A heat treatment can be applied to enhance the mechanical properties [7]. Finally they are crimped on the catheter for the deployment. Clinician during preclinical planning select the proper size of the stent and define the procedure that will be followed during implantation phase.

Additive manufacturing (AM), allowing the production of customized biomedical prostheses, is now widely used in orthopaedics applications. The cardiovascular field is still an unexplored but promising candidate for exploiting the potentialities of patient-specific devices. Through this technology, it is possible to fabricate components with high geometrical freedom starting from a metallic powder [8]. Hence, in dealing with stents, AM opens to the opportunity to directly fabricate stents that better fit the artery morphology, enabling the possibility of realizing custom-made devices to reduce the issues related to standardized ones.

Selective laser melting (SLM) is one of the most well-established additive techniques, and it consists of a laser beam that selectively melts consecutive layers of metal powder to build the designed component. Due to its high spatial accuracy and resolution, it is the most appropriate technology to be adopted in the fabrication of stents, that are characterized by micrometric features [8,9]. In addition to the geometrical freedom, SLM provides the advantage of the possibility of manufacturing multiple stents with different customized geometries at the same time, increasing productivity, and, differently by the traditional laser cutting technique, no scraps are produced [10].

Manufacturing self-expanding NiTi stents by SLM is far to be considered an easy task since many are the criticalities to be faced when dealing with such small devices. Indeed, the characteristic dimensions of the process (the laser spot diameter and the powder particle size) are in the same order of magnitude as the features of the stent's struts [8]. Currently, in the literature, there are few examples of cardiovascular stents realized by SLM. Demir et al. [8], Finazzi et al. 2019 [11] and Finazzi et al. 2020 [12] produced cobalt-chromium balloon-

expandable coronary stents, Wessarges et al. [13] used stainless steel for a similar application, and Wen et al. [14] pure zinc powder, for a biodegradable stent. All these works encountered the issue of producing closed-cell geometries due to the restrictions of the SLM process. As a matter of fact, for better flexibility and self-adaptation to the implantation site of the produced stent meshes, open-cell geometries are preferable. Indeed, open-cell stents are characterized by a reduced number of links between consecutive cells along the axial direction, and this determines higher flexibility of the device. The traditional support structures inserted during SLM manufacturing have dimensions that are comparable to those of the stent struts, and their removal by mechanical interventions might be precluded without damaging the device. Cooper et al. showed contact-free support structures for large overhangs, where the unmelted layers were left between the supports and the built part [15]. However, the building of material without any connection to the previous layers in the case of open-cells renders the use of such strategy more difficult. Hence, dedicated processing strategies should be developed.

In addition to the geometrical issues, NiTi alloys are very difficult materials to be processed by additive manufacturing in general and SLM in particular, since they are highly sensitive to variations of chemical composition [16–18]. During the SLM of NiTi, several phenomena changing the alloy chemical composition may occur, making difficult to maintain the superelastic properties after SLM [19]:

i. Nickel loss by evaporation. The high energy provided by the laser to the powder bed not only makes the metal powder melt, but also evaporates. Ni evaporation starts at 2913°C, while Ti boiling point is 3287°C. Thus, the equilibrium vapor pressure of Ni happens to be much higher than the one of Ti, and an increment of Ni loss is expected with increasing energy density. The outcome of this phenomenon is the reduction of the Ni quantity [19–24].
ii. Ni-rich precipitations. During the build process, the fabricating part is heated up due to the thermal energy transferred from the top surface, hit by the laser, to the bottom one, acting as a heat sink, generating a heat-affected zone in between. In Ni-rich NiTi alloys, precipitation of Ni-rich phases, in particular Ni_4Ti_3 precipitates, as long as Ni_3Ti_2 and Ni_2Ti, may occur at temperatures as low as 200°C, providing two main

effects: the reduction of the Ni quantity in the alloy and the reduction of ductility (since the fine particles precipitate at the grain boundary, blocking the propagation of dislocations) in the final part [24–27].

iii. Impurity pickup. During the SLM process, oxygen may be picked up reducing the Ti content in the matrix and increasing the Ni fraction. The resultant transformation temperatures can decrease due to an increased Ni content in the matrix [28].

Several works studied the shape memory effect in SLM produced parts, both in compression [25,27,29–43] and in tension [23,26,35,44,45], while some others studied the superelastic behaviour of NiTi parts produced by SLM [20,23,25,34,39,41,46–48]. Those studies enlightened that to achieve superelasticity after SLM, thermal treatments are required. The targets of the heat treatments should be the relief of the residual stresses induced by SLM and the reabsorption of the Ni-rich precipitates to re-establish the Ni content of the alloy and to increase the ductility. Moghaddam et al. [46] showed superelasticity of SLM produced NiTi specimens at room temperature without any post-process heat treatment, by fine-tuning the process parameters. However, the study of producing NiTi thin struts with adequate transformation temperatures in the view of stenting remains an open field.

Finally, another barrier to be overcome in the realization of NiTi stents by SLM is the very low thickness of the struts, that is comparable to the laser beam diameter. As demonstrated by Caprio et al. [49], pulsed wave (PW) SLM systems are more suitable for the production of fine geometries, thus they have to be preferred to continuous wave (CW) systems in the case of this work. However, all the studies that were cited in the previous paragraph about SLM of NiTi employed CW systems, since it is more common than PW ones. Recent works [50–52] showed the capabilities of PW emission for producing NiTi lattices structures. While the use of PW for moving towards very thin struts (<0.5 mm) typically used for stenting applications is yet to be developed.

In light of all these current limitations, the geometry of the device and the process-related parameters should be studied to reach satisfactory, reliable, and repeatable results [11]. This work investigates the feasibility of manufacturing a NiTi stent with a novel open-cell mesh and variable diameter by SLM, moving the first step to the realization of patient-specific devices to treat PAD. A dedicated build strategy and process parameters study

was proposed to obtain the desired geometrical features, together with adequate density and thermo-mechanical properties.

2. Materials and methods

2.1. Design of the NiTi stent mesh with open-cell and variable diameter

The main restriction to design stents by SLM regards the overhang and unsupported regions that normally require support structures. Hence, building the stent along the vertical direction without overhangs and unsupported regions employing an adequate design is a straightforward approach. However, in this way, the production of stents with open-cells is not viable. Open-cell stents are characterized by a reduced number of connections between the adjacent peaks and valleys of the mesh, which translates into the presence of local minima not mechanically linked to an already built part of the component. Without the use of support structures, these regions should be built on loose powder.

In order to produce open-cell stent meshes, the adopted strategy in this work was based on leaving small gaps in the build direction between adjacent peaks and valleys of the open-cell mesh. The mesh was designed such that the peaks and valleys are separated only by a low number of layers of not-melted metal powder. However, during SLM, the melt pool can penetrate several layers. The idea was to exploit this phenomenon for the generation of thin and weak links between the lower and the upper struts of two adjacent rings. These bridges should be robust enough to reliably support the growth of the upper part of the device, but they should also be weak enough to be easily removable via post-processing such as ultrasonic cleaning, electropolishing, or chemical polishing. Resultantly, the cells can be opened up by the end of the process chain.

In order to test the feasibility of the approach, a novel stent mesh for SLM was designed. It has an open-cell configuration with Z-shaped cells, which is commonly used in commercially available peripheral cardiovascular stents. The CAD model of the stent followed a similar workflow of the stents produced by laser cutting. The mesh was drafted in 2D, then wrapped on a tubular element, and the cells (i.e. the closed profiles) were cut through the

tube wall. Figure 1 shows the elementary unit of the mesh represented together with the 3D model. The unit mesh was made of two equal cells having two orthogonal axes of symmetry and their sides equally sloped. The elementary unit was replicated multiple times to obtain the global mesh. The stent was designed with variable diameter suited for the arteries of the peripheral system. The stent started with a diameter of 8 mm, reached 7 mm along the sloped stretch of the tube, and terminated with 6 mm. The nominal strut thickness was 180 µm with a length of 6 mm. All the dimensions that are parallel to the build direction were chosen as an integer multiple of the 30 µm layer thickness adopted for the build [11]. The gap between the open-cells was parametrically designed using the variable dimension 'cell gap' (*CG*) and set at integer multiples of the layer thickness.

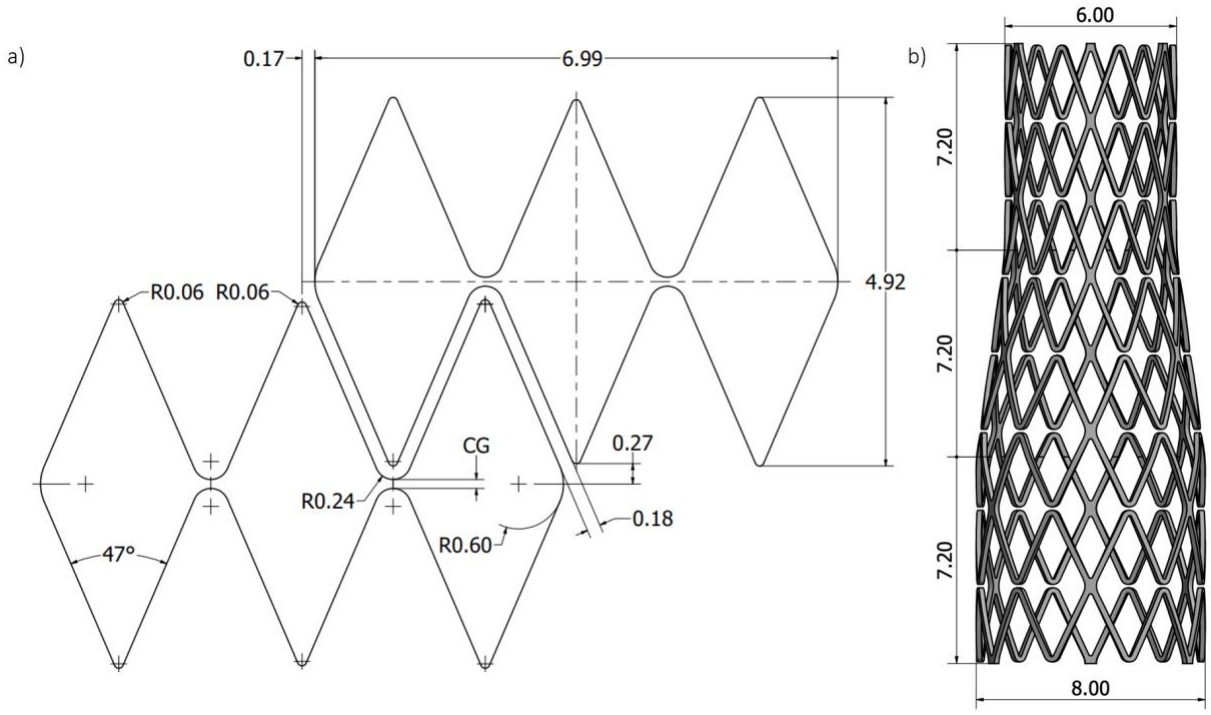

Figure 1. The novel stent mesh. a) The elementary unit composing the stent mesh with variable cell-gaps (*CG)*, b) 3D CAD model of the open-cell stent with variable diameter.

2.2. NiTi powder

The NiTi powder had a nominal composition of the alloy $Ni_{50.8}Ti_{49.2}$, and it was obtained through gas atomization, for particles that have a diameter <45 µm (provided by SAES Getters SpA, Lainate, Italy). The powder was characterized by a limited fraction of impurities concerning 605 ppm C and 1254 ppm O. The powder feedstock

had an austenitization finishing temperature at 16°C, rendering it feasible as a superelastic NiTi feedstock. Figure 2 shows the scanning electron microscopy (SEM) image of the powder.

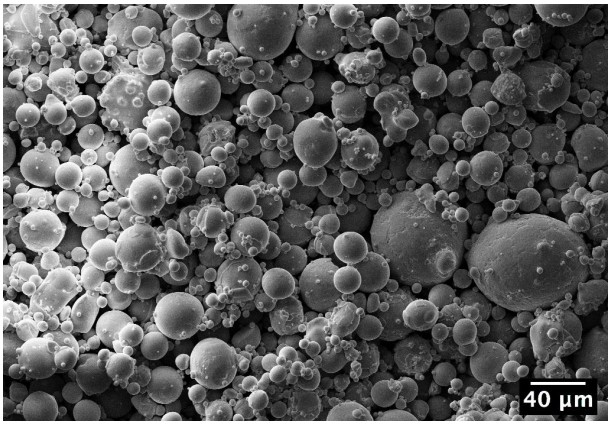

Figure 2. SEM image of the NiTi powder employed in the present work.

2.3. Selective laser melting system

An industrial SLM machine (Renishaw AM250, Stone, UK) was employed with a reduced build volume (RBV) ancillary, which reduces the available build volume to 78x78x50 mm^3. The machine is equipped with a single-mode fiber laser (R4 from SPI, Southampton, UK) able to deliver a maximum power of 200 W through an optical chain that results in a laser beam diameter of 75 µm at the focal point. The laser source operates in pulsed mode (PW), and it can generate µs-long pulses by power modulation. For all the experiments of the current work, the build chamber was kept under a controlled atmosphere, filled with Ar operating at <1000 ppm of O_2.

2.4. Characterization equipment

Optical microscopy was used for acquiring images of the struts to measure the strut dimensions and the apparent density observing the longitudinal cross-sections with an image processing software (ImageJ, Bethesda, USA). SEM was used to observe the strut and stent morphologies (EVO-50, Carl Zeiss, Oberkochen, Germany). Differential scanning calorimetry (DSC) analyses were carried out to evaluate the effect of the SLM process and the heat treatments on the transition temperatures of the NiTi alloys (DSC2000 TA Instruments, Dallas, TX, USA). A single cycle was applied between -150°C and 150 °C in order to avoid the effect of multiple thermal cycles

especially on the as-built samples. The results were plotted between -80°C and 80°C for better identifying the baseline. Energy Dispersive X-Ray analyses were performed on as-built samples to support the DSC ones in the evaluation of the effect of the SLM process parameters on Ni content variation (INCA crystal, Oxford Instruments plc, Abingdon-on-Thames, United Kingdom). EDX measurements were taken at five distinct points on with a sensing depth of up to 5 µm and considering Ni and Ti only.

3. Process development for producing NiTi stents by SLM

3.1. Processing of thin NiTi struts

As starting point, the SLM process parameters were studied to produce thin circular struts as elemental geometries of the stents according to the designed dimensions. The type of scan strategy can depend on the fine strut geometry required and the type of material [8,53]. It has been shown that both concentric and hatching strategies can be employed for thin struts. Through the preliminary analysis, not reported here for the sake of brevity, meander strategy was found to be more appropriate. The point (d_p) and line (d_l) distances were kept equal at 45 µm. The focal point was placed on the powder bed (f=0 mm). In this configuration, the number of pulses on the powder bed was kept fixed, while the laser power (P) and the exposure time (t_{on}) were varied between 54 and 150 W and 24 and 60 µs respectively. Both the varied process parameters were investigated with 4 levels in a full factorial experimental design. All conditions were replicated 5 times. No beam compensation was employed. Within the experimental campaign, the energy density was varied between 40 and 70 J/mm^3. Table 1 summarizes the experimental plan.

The optical microscopy images of the struts were used to measure the diameter. As shown in Figure 3, the images were processed to detect the edges and the related profile. The effective diameter d_{eff} of the specimen was calculated as the average distance between the two sides of the rotated profile. The average strut diameter error d_{err} was calculated as follows:

$$d_{err} = d_{eff} - d_{nom} \quad (1)$$

where d_{nom} is the nominal strut diameter.

Table 1. Details of the experimental plan.

Fixed parameters	**Value**
Scanning strategy	Meander
Focal position, f [mm]	0
Point distance, d_p [µm]	45
Line distance, d_l [µm]	45
Layer thickness, z [µm]	30
Varied parameters	**Levels**
Power, P [W]	54; 86; 118; 150
Exposure time, t_{on} [µs]	24; 36; 48; 60

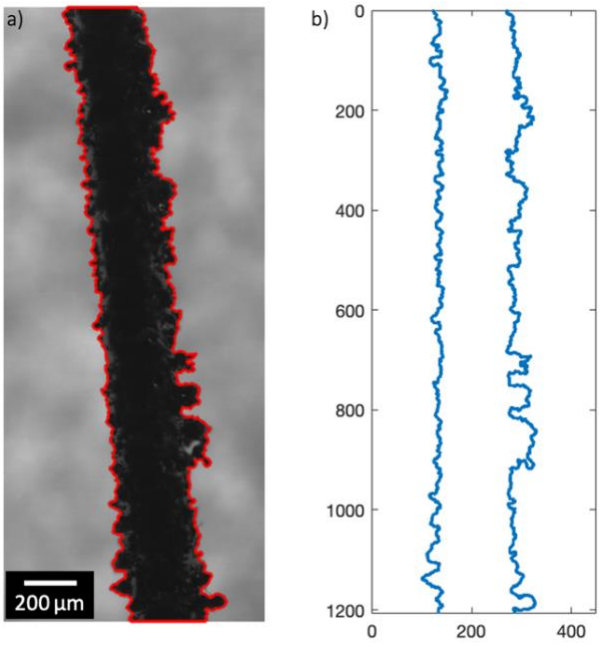

Figure 3. Extraction of the strut sample profile. a) Optical microscopy image of a strut sample with the detected profile, b) the sample profile after rotation (values in pixel).

3.1.1. Apparent density

The images of the longitudinal strut cross-sections were used to measure the apparent density. The images were binarized revealing the pores as bright regions as shown in Figure 4. The apparent density ρ was calculated with the following expression:

$$\rho = \frac{A_{tot} - A_{pore}}{A_{tot}} \quad (2)$$

where A_{tot} is the total area of the measured region and A_{pore} is the total area of the pores indicated as the white regions in the images. The cross-section analysis was preferred over the Archimedes method due to the small mass of the specimens.

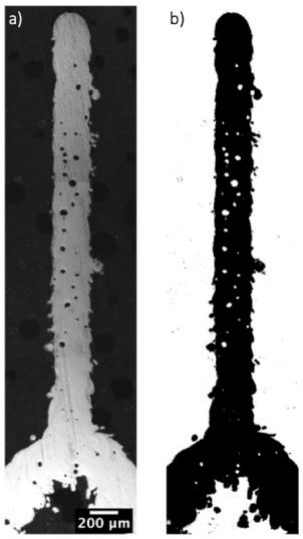

Figure 4. Cross-section of an SLM produced strut. a) Optical microscopy image, b) image after binarization.

3.2. Process development for open-cell and variable diameter stent production

As following step, the results deriving from the strut processability study were used to set the process parameters of an experimental campaign designed to assess the possibility of producing open-cell stents with variable diameter. The exposure time (t_{on}) was fixed at 60 µs. The cell gap (*CG*) was studied with 4 levels, leaving unmelted gaps of 1, 2, 3, and 4 layers between adjacent rings. The cell opening was assessed in as-built conditions as well as after an ultrasonic cleaning of 20 minutes in distilled water to break the apparently closed gaps. The power (*P*) was varied at two levels 86 and 118 W in order to assess the integrity of the process in the presence of unconnected layers. A qualitative analysis was made by observing the build stability with the investigated conditions and the success in opening the cells. Table 2 summarizes the experimental conditions.

Table 2. Details of the experimental plan for the realization of the open-cell stents with variable diameter.

Fixed parameters	**Value**
Scanning strategy	Meander
Focal position, f [mm]	0
Point distance, d_p [μm]	45
Line distance, d_l [μm]	45
Layer thickness, z [μm]	30
Exposure time, t_{on} [μs]	60
Varied parameters	**Levels**
Power, P [W]	86; 118
Cell gap, CG [μm]	30; 60; 90; 120

3.3. Transition temperatures in as-built and heat-treated conditions

An SLM process leaves internal stresses in the built components that work against its mechanical behaviour. Moreover, dealing with NiTi alloys, the high temperatures reached during the process lead to a variation in the final chemical composition and the formation of precipitates. Hence, the transformation temperatures of the SLM processed material can be different from the conventionally produced NiTi. Accordingly, DSC measurements were carried out on specimens in as-built condition, after either a solution annealing treatment or a stress relieving treatment. EDX analyses were carried out on as-built samples and on the powder to quantitatively evaluate the chemical composition of the alloy after the production process. Processing conditions with variable laser power at 86 and 118 W were investigated along with the heat treatments.

After SLM process, the samples were heat treated in order to improve the functional properties. The heat treatment conditions were set similar to what is used in industrial practice for solution annealing and stress-relieving. Solution annealing was carried out at 850°C for 30 minutes. During this treatment the recrystallization temperature of the alloy is overcome, allowing grains to grow and the Ni-rich precipitates (mainly Ni_4Ti_3) to be reabsorbed by the matrix [7,54]. This treatment is not conventionally used in NiTi stents as a part of the heat treatments successive to the laser cutting operation. Such treatment may generate excessively enlarged grains and can be employed after

the casting alloy prior to the successive plastic deformation processes such as extrusion and drawing. In the case of SLM produced stents, solution annealing constitutes the basis for evaluating the amount of Ni loss. Stress-relieving was carried out at 450°C for 15 minutes. With this treatment, significant grain growth is potentially suppressed, while the residual stresses generated due to the fast-cooling cycles are resolved, similar to what is done for cold worked NiTi [7].

For the transition temperature study, dedicated flat meshes having the same stent geometry were produced according to the experimental conditions summarized in Table 3. Three replications were produced for each case. The samples were analysed with the DSC equipment following the ASTM F2005 standard, with an imposed variation of temperature of 10 K/min between -150°C and 150°C. The DSC analysis provided the austenitic transformation peak and the martensitic transformation peak temperatures (A_p and M_p), as well as the austenitic transformation finish and the martensitic transformation finish temperatures (A_f and M_f).

Table 3. Details of the experimental plan for the characterization of the transition temperatures.

Fixed parameters	**Value**
Scanning strategy	Meander
Focal position, f [mm]	0
Point distance, d_p [μm]	45
Line distance, d_l [μm]	45
Layer thickness, z [μm]	30
Exposure time, t_{on} [μs]	60
Varied parameters	**Levels**
Power, P [W]	86; 118
Condition	As-built
	Solution annealed @800°C x 30min
	Stress relieved @450 °C x 15 min

4. Results

4.1. Processability of thin NiTi struts by SLM

4.1.1. Strut diameter

Figure 5 shows the SEM images of the as-built NiTi struts. As the laser power and exposure time increases the struts become more regular and larger in diameter. The surface irregularity at low power and low exposure time is

constituted by the irregularly formed melt pools, while at higher power and higher exposure times the loosely adhered powder particles appear as the main surface feature corresponding to irregularity.

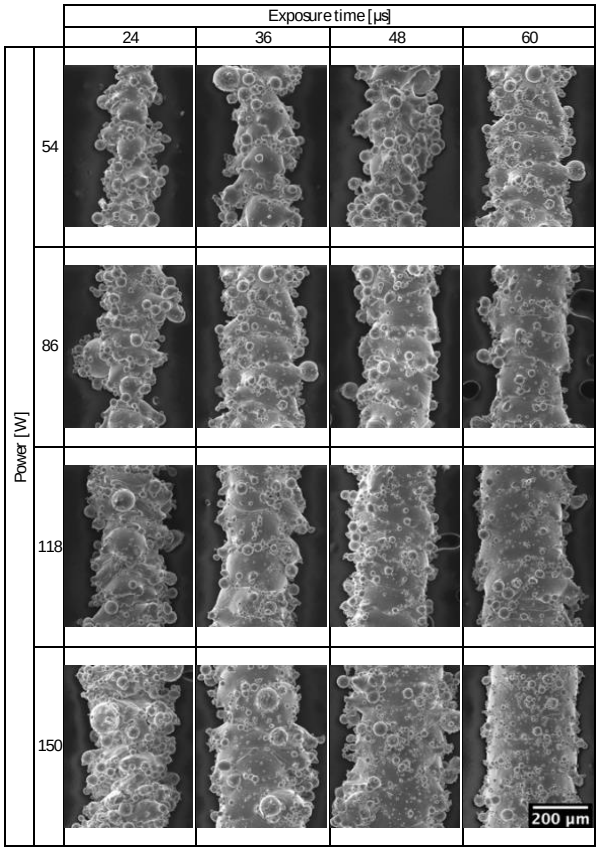

Figure 5. SEM images of the NiTi struts as a function of the process parameters.

The strut sizes varied between 170 to 320 µm in the experimented conditions corresponding to values lower and higher than the nominal dimension. It can be expected that the negative diameter errors are a sign of insufficient energy provided to the powder bed in the least energetic condition (P=118 W, t_{on}=24 µs). Figure 6 shows diameter error as a function of the process parameter. The diameter error follows a clear trend of increase as the energetic conditions are increased. The largest error corresponds to approximately 75% of the nominal diameter. The use of beam compensation in the experimented cases is not a viable option as it is comparable to the size of the strut. Instead, the strut thickness should be designed to considering the diameter error of the SLM process to achieve the desired dimension by the end of the additive manufacturing process. Moreover, the diameter error can be considered similar to the melt pool size in absence of the beam compensation. Accordingly, within the examined

parameter combinations, the melt pool size is varied below and above the beam diameter (75 µm). Despite the diameter errors observed, the strut sizes achieved are in the range of the conventional NiTi stent struts, which confirms the efficacy of the pulsed wave emission in the greater control over the melt pool dimension and hence the produced geometry [9].

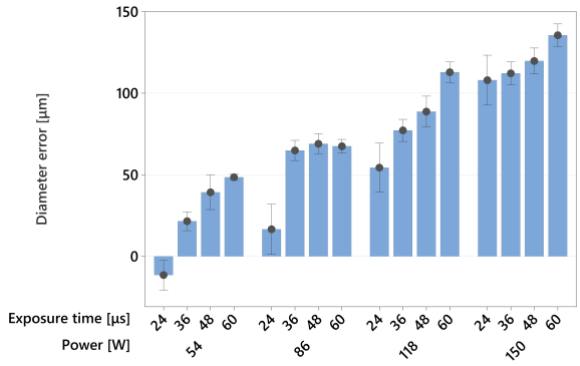

Figure 6. Diameter error as a function of exposure time and power.

4.1.2. Apparent density

Figure 7 shows the longitudinal sections of the produced struts. With the 24 µs exposure time the specimens were thin and loosely adhered rendering the cross-sectioning process difficult. A single condition within this irregular region (P=118 W, t_{on}=24 µs) could not be analysed in further detail due to failed specimens during the build and the polishing stage. Indeed, the cross-section images show that the process stability in terms of geometrical well-defined and dense struts is achieved above 24 µs of exposure time. At 24 µs exposure time, the lack of adherence between the layers is similar to a lack-of-fusion porosity. The pulse duration can be too low for a stable emission of the laser source, which can emit a minimum of 20 µs long pulses at full power [55]. It is known that fiber lasers may have emission delays and ramped emission profiles, which may be longer with low power levels [49,56]. With 24 µs pulses and lower power levels it can be expected that the laser may not reach the desired power level, hence lowering the effective energy input. The geometrical profile is more stable with higher powers at 118 and 150 W. This is coherent with the surface topography observations through the SEM images seen in Figure 5. In the experimented conditions, the types of pores observed are spherical, indicating a possible gas entrapment.

Beyond a reduction of the mechanical properties, the generation of gas pores can indicate Ni loss and hence a change of the transition temperatures.

Figure 8 shows the measured apparent density of the struts as a function of laser power and exposure time. Both the parameters have a strong influence on the densification. At 86 W laser power all exposure times allow achieving density values higher than 99%. At 118 and 150 W an increase of exposure time relates to reduced density accompanied by larger pores. The measurements underline the sensitivity of the material to the energy input in the given small dimensions leading to a small processability window where geometrical integrity and porosity can be maintained at acceptable levels. The apparent density did not follow a clear trend against the energy density, which is not reported in the work for brevity. This is expected to be due to the marked influence of the single parameters, which is not explainable by an aggregate energy density parameter.

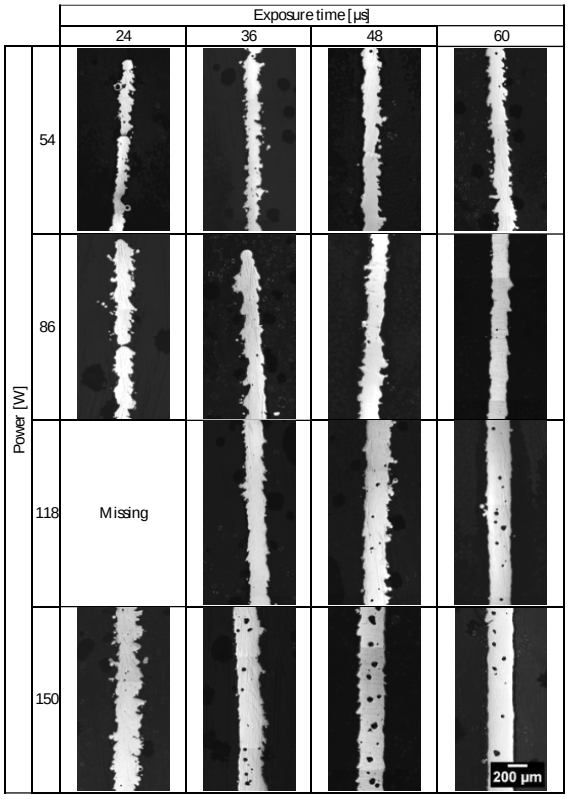

Figure 7. Optical images of NiTi struts longitudinal sections as a function of the process parameters. The material porosity is strongly affected by the combination of exposure time and power

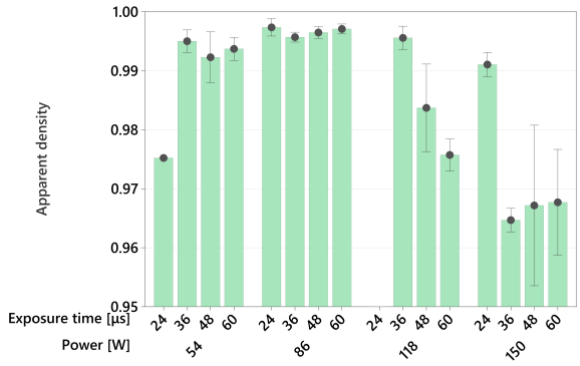

Figure 8. Apparent density of the NiTi struts as a function of exposure time and power.

4.2. Processability of the NiTi stents with open-cell and variable diameter

Once the feasible conditions for producing vertical struts were established, stents with open-cell and variable diameters were produced with fixed exposure time at 60 µs and power levels varied at 86 W and 118 W. Figure 9 shows the produced stents around the separation zones of the open-cells. A single layer of *CG* (30 µm) appears inadequate for successive separation by means of ultrasonic cleaning independently from the laser power employed. It can be expected that the laser energy is sufficient to penetrate through a single layer generating a strong link. With *CG* above a single layer, the cells were successfully opened after ultrasonic cleaning. With 4 layers of *CG* (120 µm) instead, the cells were open in the as-built condition. Furthermore, higher laser power generates an extended penetration depth. Hence, after ultrasonic cleaning with 118 W laser power and cell gap with more than 1 layer, the linking zones remain close to contact. On the other hand, after ultrasonic cleaning with 86 W laser power and cell gap with more than 1 layer, the linking zones remain with a gap close to the un-melted layer number. Figure 10 shows an example of SLM produced NiTi stent with open-cells and variable diameter employing 118 W laser power and 3 layers of gap (90 µm) between the open-cells. The geometry is produced with high fidelity and the cells are open after the ultrasonic cleaning. The high surface roughness due to melt morphology remains an open issue to be studied via the post-processing methods.

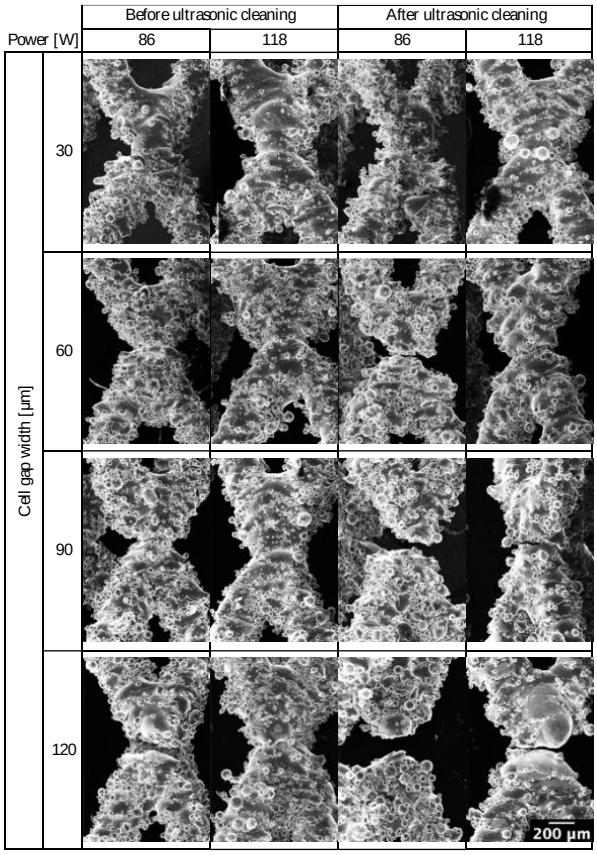

Figure 9. SEM images of the separation zones of the stents with open-cells produced with different cell gaps and power levels, before and after the ultrasonic cleaning procedure.

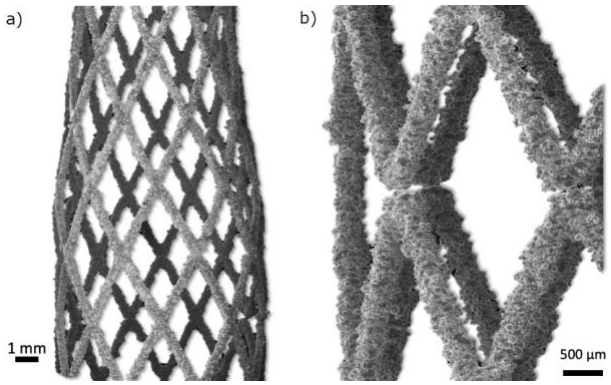

Figure 10. a) SEM images of an SLM produced NiTi stent with open-cells and variable diameter employing 118 W laser power and 3 layers of gap between the open-cells, b) detail of the separation zone of the open cells

4.3. Transition temperatures

Figure 11 shows the typical DSC curves for a flat mesh sample in the as-built, solution annealed and stress relieved conditions, compared to the one of the NiTi powder. The peak found along the heating curves identify the transition between martensitic/cold phase of the NiTi alloy and the austenitic/hot one, that is an endothermic transformation, while the peak found along the cooling curves identify the reversed transformation, that is an exothermic transformation [57]. The as-built material shows the transformation peaks despite they are not well defined indicating small transition enthalpies, and in accordance to literature [22] both the martensitic and the austenitic transformations are shifted to higher temperatures with respect to the initial powder after the SLM production process. The heat treatments tend to change the position of the transition peaks and finishing points. Stress relieving better defines the transition peaks, increasing the transformation enthalpy especially of the martensitic transition, however it usually introduces double peaks possibly due to the presence of the R phase along the cooling path [58]. On the other hand, the solution annealing treatment tends to lower the transformation enthalpy of the samples with respect to the as-built condition, sometimes making it difficult to actually recognize the transition peaks.

Figure 12 shows the results of the tests performed on 3 samples for each treatment and power, in terms of austenitic and martensitic transformation peak temperatures. It should be noted that not all the transformation temperatures were revealable on all the DSC curves, such as M_f after the stress relieving treatment. Figure 13 depicts the finishing temperatures for the austenitic and martensitic transformation. In Table 4 are summarized all the temperature data and the measured austenitic and martensitic transformation enthalpies ($H_{M\rightarrow A}$ and $H_{A\rightarrow M}$). The data reveal that both the laser power and the heat treatment condition play an important role in the transition behaviour. In particular, the austenitic finish temperature is the critical indicator of superelastic functionality. In principle, A_f should be lower than the room temperature for generic applications and less than the temperature of the human body (37°C) for the biomedical ones. The A_f of as-built samples is widely affected by the laser power, where with higher laser power A_f rises above the body temperature. It should be noted that due to the not well-defined shape of the DSC curves reliable temperature data concerning A_f and M_f could not be retrieved, and the results should be

considered indicative. Solution annealing allows the Ni precipitates to be reabsorbed and the stresses to be relieved. Hence, in this condition the transition temperatures can be comparable to conventional NiTi alloys, as the temperature variations could be attributed to only chemical composition variation such as Ni loss, O or N pickup. After solution annealing, the A_f of the 118 W specimens remains at higher temperatures. It can be expected that at a higher fraction of Ni is lost when the power is increased from 86 W to 118 W. Although the observed transition temperatures after solution annealing for both the power levels are appealing for superelasticity, the prolonged solution annealing may generate larger grains and reduced mechanical resistance [54,59]. On the other hand, the stress-relieving treatment appears to be insufficient in maintaining A_f below the body temperature. It can be deduced that the stress relieving treatment may not be able to relieve the internal stresses as well as dissolving the Ni precipitates of the SLM produced NiTi stent meshes. The transition enthalpies vary between approximately 8 and 20 J/g from martensite to austenite and 5 to 10 J/g from austenite to martensite. The transition enthalpy can be also further interpreted for shape memory effects and the intensity of the transformation. Overall, the measured values are moderate for martensitic and austenitic transformations.

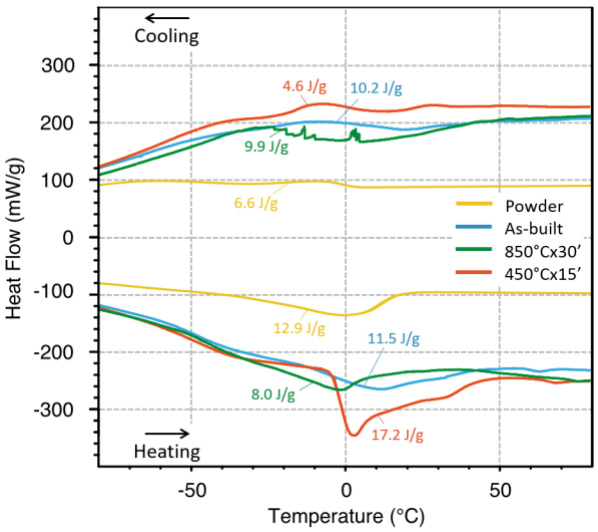

Figure 11. DSC graphs of a flat mesh sample in the as-built, solution annealed and stress relieved conditions (P=118 W), as well as the one of the NiTi powder.

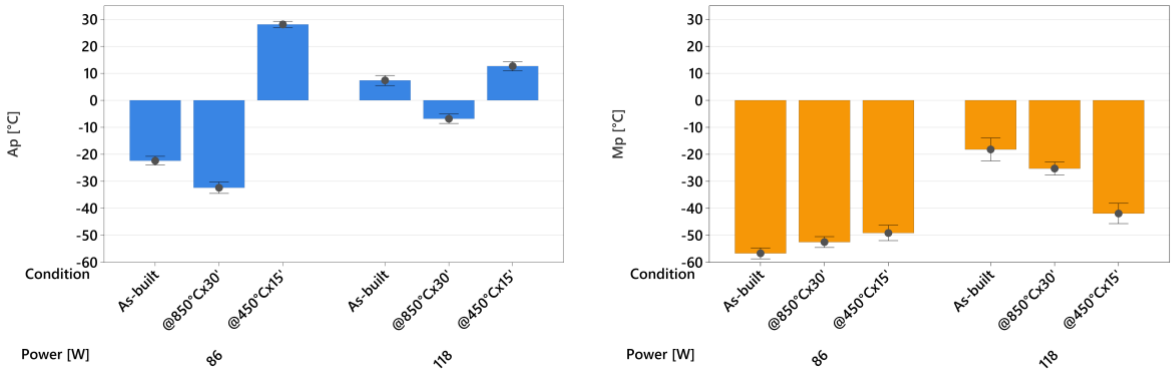

Figure 12. Austenitic transition peak (A_p) and martensitic transition peak (M_p) temperatures of the investigated conditions.

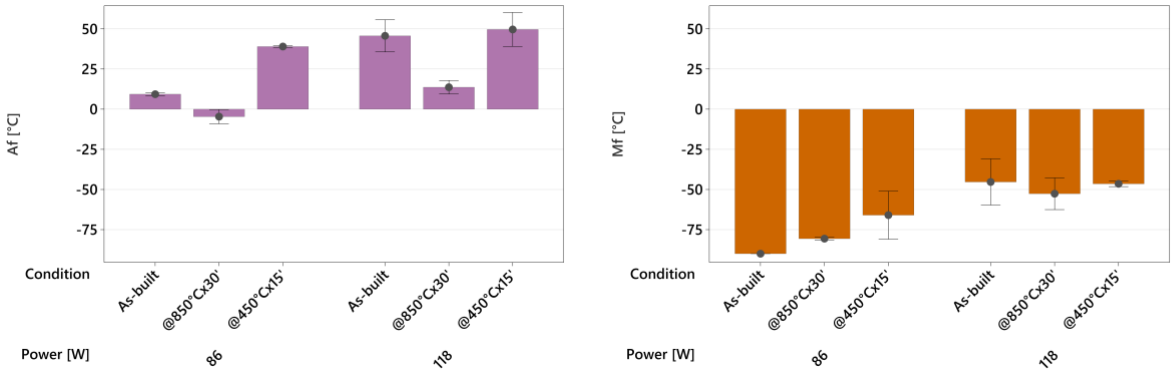

Figure 13. Austenitic transition finish (A_f) and martensitic transition finish (M_f) temperatures of the investigated conditions.

Table 4. The main transition temperatures as a function of the laser power and heat treatment, as long as the transformation enthalpies (results are show as mean ± standard deviation).

Laser power (W)	**Heat treatment**	**A_p (°C)**	**M_p (°C)**	**$H_{M\rightarrow A}$ (J/g)**	**A_f (°C)**	**M_f (°C)**	**$H_{A\rightarrow M}$ (J/g)**
86	As-built	-22.4±4.6	-56.7±3.5	16.4±0.1	9.3±1.5	-90.0±1.0	6.4±0.0
86	850°Cx30’	-32.4±5.9	-52.5±4.0	9.0±2.5	-4.7±6.6	-80.7±1.2	5.0±0.4
86	450°Cx15’	28.1±3.5	-49.1±8.0	9.5±2.7	39.0±1.0	-66.0±18.4	6.5±1.3
118	As-built	7.4±6.2	-18.2±13.3	11.8±0.5	45.7±15.0	-45.3±21.6	8.2±2.1
118	850°Cx30’	-6.8±5.8	-25.3±7.9	8.2±0.7	13.7±6.4	-52.7±14.8	8.5±1.8
118	450°Cx15’	12.6±5.8	-41.9±12.4	18.5±1.5	49.7±15.9	-46.5±2.12	9.8±5.4

4.4. Chemical composition

Table 5 shows the Ni content measured by EDX. The EDX measurements reveal a lower average Ni content with respect to the nominal one with a large confidence interval. It should be noted that an error margin of 1 at% is

common to the EDX measurements. In the EDX measurements oxygen content was included. The low atomic mass of the element provides usually high inaccuracies with EDX. Moreover the EDX measurements remain superficial, hence a higher oxygen fraction can be revealed due to the surface oxides. Hence the evaluation of the chemical composition and its influence on the final transformation temperatures requires further considerations.

First, the average Ni contents revealed by EDX should be considered between the measurements to reveal whether any statistical difference exist. One-way analysis of variance (ANOVA) confirmed that EDX measurements of the powder, *P*=86 W and *P*=118 W conditions were not statistically different (p-value=0.99). At this point the confidence intervals can be compared to the nominal powder Ni composition. It is noted that the nominal Ni content is within error margin of the measurements (in particular within the confidence intervals). Hence, it is not possible to conclude that during the SLM process a significant Ni depletion should have occurred.

The difficulty of measuring the exact chemical composition is often resolved inversely by matching the transformation temperatures with the known chemical compositions. The material should be in a solution annealed state with all NiTi precipitates resolved into the matrix. In this condition, the measured transition temperatures, and especially A_f depends on the Ni content as well as the level of oxidation. Frenzel et al. [28] described an empirical model to predict the transition temperatures by including the impurities in the NiTi alloy such as oxygen. The model calculates the true Ni content in the NiTi matrix as oxygen and carbon will reduce the Ti content as chemically bonding to this element. Hence the model estimates increased transition temperatures with a decrease of the nominal Ni content and with an increase in the O content. The model was used to estimate the range of Ni depletion and oxygen pickup within this work. The austenite finish temperature (A_f [°C]) was calculated using the following expression:

$$A_f = \left(A + B x_{Ni}^{p,O,C} + CD^{\left(x_{Ni}^{p,O,C} - 50\right)}\right) - 273 \quad (3)$$

where, *A*=4954.34606, *B*= -91.49629, *C*=-0.13819, and *D*=86.75202 are experimental coefficients and $x_{Ni}^{p,O,C}$ is the true Ni concentration using the following expression

$$x_{Ni}^{p,O,C} = \frac{1 - x_O - x_C}{1 - 7x_O - 2x_C} x_{Ni}^{P} - \frac{2x_O}{1 - 7x_O - 2x_C} \quad (4)$$

Where x_O, x_C, and x_{Ni}^{P} are are carbon, oxygen and Ni concentrations in at% respectively. The model was employed to estimate nickel and oxygen content ranges in the SLM built specimens using the A_f ranges (mean ± standard deviation) in the solution annealed condition. Ni content was considered at the minimum average of 50.1 at% and the nominal 50.8 at%. Carbon content was neglected as during the SLM process its pickup expected to be less dominant compared to oxygen. The oxygen content was considered between 0 at% and 0.9 at% tentatively. The model results are plotted in Figure 14. In order to confirm the accuracy of the model, the declared powder chemistry was used to estimate the A_f value. The result was satisfactory close to the measured one with DSC (estimated A_f=12.5°C indicated as "powder declared" in Figure 14). Using the EDX measured Ni content (50.1 at%) and the DSC measured A_f (16°C) of the powder, instead the oxygen content was calculated at 0.76 at% (indicated as "powder EDX" in Figure 14). The calculations on the powder chemistry shows that the inaccurate measurement of Ni content via EDX may indicate an increased amount of oxidation in the calculations. With these considerations in mind, the chemical composition of the SLM processed NiTi specimens should be evaluated within an uncertainty band as shown in Figure 14. It can be seen that the expected oxidation levels can be higher than the initial one between 0.1-0.8 at%. During the SLM process, the remaining oxygen content in the process chamber can be expected to be picked up, accompanied by a very limited amount of Ni depletion. It can be seen that the conditions with the higher power level maintain the A_f with respect to the powder feedstock, while the lower power level shows a reduced A_f. With a higher laser power, it can be expected to have a higher degree of Ni depletion. Instead with a lower power level, it can be expected that oxidation is the dominant factor in the change of the chemical composition. Indeed, Ti oxidation starts at a much lower temperature (550°C) compared to Ni evaporation (2913°C) [60]. Under the light of these considerations, it can be concluded that in the tested SLM conditions Ni depletion was accompanied by oxygen pickup counterbalancing the losses. As a matter of fact with the lower power level oxygen pickup was the dominant factor reducing the A_f.

Table 5. Nickel content measurements (results are show as mean ± 95% confidence interval for the mean).

Condition	Ni at%
Powder nominal	50.8
Powder EDX	50.1±0.9
P=86 W	50.2±0.6
P=118W	50.2±0.5

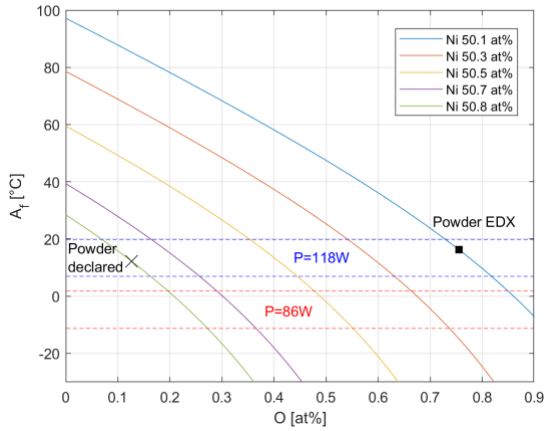

Figure 14. Influence of oxygen and nickel content on A_f calculated using the empirical model from Frenzel et al. [28]. The horizontal bands indicate the A_f ranges for the two power levels (mean ± standard deviation). The "powder declared" condition shows the estimated A_f with the declared chemical composition. The "powder EDX" condition shows the estimated oxygen level using the DSC measured A_f and EDX measured Ni content.

5. Discussion

Within this study, the processability of open-cell NiTi stents with variable diameters was investigated. Our investigation sheds light on the interplay between the stent design, process parameters, and the consecutive heat treatments for the correct functioning of these devices. The results showed that a small processability window is present for achieving high density along with good geometrical fidelity. From this perspective, moderate power (86 W) and exposure times (60 µs) are appropriate. Higher power levels were found advantageous for the geometrical fidelity, while the use of high power can render the opening of the cell links more difficult. Finally, the transformation behaviour was found to be closely related to the processing conditions and applied heat treatment. As desired, after solution annealing, the austenitic transformation finish temperatures were lower than the body temperature. The higher power levels indicated a lower fraction of Ni as observed by the higher A_f. The

processed alloy has nominally A_f at approximately 16°C. After the solution annealing, the A_f appears to be comparable to that of the powder feedstock. A slight reduction can be associated with oxygen and nitrogen pickup during the process reducing the Ti fraction in the alloy matrix. Despite working under the Ar atmosphere, a minimum fraction of oxygen remains in the process, which may bond to the processed alloy in the melt pool. Overall, the results indicate that the SLM-produced struts appear to possess the correct chemistry. Although several works have studied the processing of NiTi by SLM, the comparison of transition behaviour is a difficult task due to the differences in the initial chemical compositions, processing conditions and the geometries tested. Speirs et al. [22] observed significant Ni depletion (0.2-0.6 at%) as a function of the process parameters employing powder feedstock with 50.6 at% Ni. The consequent A_f levels appeared to be higher than room temperature after solution annealing. The authors showed that a relatively higher oxygen content (1800 ppm) in the processing atmosphere allowed to reduce A_f after solution annealing. It can be expected that Ni depletion accompanied with Ti oxidation can maintain the required composition in the matrix adjusting the final transition temperatures. Saedi et al. [48] processed NiTi powder with 50.8 at% Ni. The authors observed sufficiently low A_f levels in as-built and solution annealed conditions. The authors also tested the specimens in compression at A_f+15°C observing superelastic behaviour upon designated aging treatments. Recently Wang et al. [61] showed SLM of NiTi with a 50.6 at% Ni content. The authors observed an overall increase of A_f with the increase of energy density, which was mainly associated with the preferential Ni loss. The authors observed a similar issue concerning the strong influence of the process parameters on both the density and the transition temperature. In this work, the density along with the required transition temperatures could be achieved with very fine geometrical details required for the stenting applications. The careful adjustment of the processing parameters were found to be vital for avoiding excessive Ni depletion and moving towards functional medical devices produced by additive manufacturing. The chemical composition measurements also indicated that excessive Ni depletion is unlikely, while slight oxidation during the SLM may have helped maintaining low austenitic finish temperatures. The overall results underline the high sensitivity of the NiTi alloy to the chemical composition variations. A combined effect of Ni depletion with oxidation during the process is expected to generate the final A_f level. While the measurement uncertainty remains

an important factor for the determination of the exact chemical composition, it can be concluded the PW emission is effective in terms of maintaining the chemical composition of the NiTi. The atmospheric control during the SLM process remains an open point for further investigations. During the process the oxygen amount varies due to a cyclic oxidation and oxygen release. In the initial phase, the process chamber has a remaining amount of oxygen (<1000 ppm in this work). In the initial layers, this amount can be used for oxidising the material. In the following layers, the oxygen is expected to be released due to the melting of the feedstock, which will inherently have an oxide layer. It can be deduced that the material composition may vary during the build of successive layers. The initial oxygen content as well as the gas type are fundamental for the control of the final material chemistry and hence the transition temperatures.

Clearly, in order to evaluate the performance of the stent, it is necessary to carry out inspections regarding the actual mechanical properties. One of the critical points regards the testing of the thin struts. The process produces struts with high surface roughness and irregularities increasing the geometrical variability. Hence, next step will be the set-up of a surface finishing process both for roughness reduction and adjusting the strut thickness. A thorough investigation of the surface finishing will be performed, combining chemical and electrochemical techniques. Once a regular geometry will be achieved it will be possible to perform experimental tests and evaluate the superelastic behaviour of the material. In case, tailored heat treatments will be studied to improve the mechanical performance according to the requirements related to the PDA stenting application. Surface roughness can be influential on the superelastic behaviour as the surface imperfections can impede the deformation.

Another advantage of SLM stent production is the possibility of obtaining stent struts with variable thicknesses. However, this feature require a careful evaluation in terms of the correct disposition of the laser pulses in the thickness variations as well as in terms of very accurate control of the finishing process. Further advantages of the additive manufacturing process can be obtained also via topological optimization procedures to produce patient-specific devices. These points will be subjects of future studies.

6. Conclusions

This work showed the design and SLM of a novel open-cell stent mesh with variable diameter for superelastic NiTi stents. The work shows a methodological approach from process parameter selection to the characterization of transition behaviour. In particular, the work aimed at maintaining high density, good geometrical fidelity and reasonable transition temperatures for use in peripheral stents. The main outcomes can be summarized as follows.

- A novel stent cell mesh with an open-cell design and variable diameter was designed for production by SLM. The novel mesh aimed to go beyond the existing limitations of the design for SLM and exploit the existing freedom for patient-specific stents design for the personalized treatment of the pathology.
- The process parameters were studied to achieve pore-free struts with geometrical fidelity starting from a feedstock with 50.8 at% Ni (A_f=16°C). The experimental work showed that the processability window is limited. The geometrical integrity improved with an increase of porosity due to the plausible entrapment of evaporated Ni.
- Cell struts could be opened via the employed support-free build strategy. By adequately choosing the number of layers for the cell gap, stents with open-cells could be achieved after ultrasonic cleaning. Further chemical and electrochemical processing are expected to be of aid to also better open the cell links.
- The transformation behaviour of SLM produced NiTi was analysed via DSC analysis, in as-built, solution annealed and stress relieved conditions. The solution annealing showed that the chemistry of the produced NiTi struts is adequate (A_f<37°C). The stress-relieving was not able to retrieve the transformation temperatures to the expected levels.
- The use of high-quality feedstock with the correct manipulation of the process parameters is found to be vital to suppress excessive Ni depletion and to maintain a homogenous transformation behaviour. The interplay between oxygen pickup and Ni release are expected to be determinant on the final transition temperatures as well as the heat treatments applied.

The present work identified a possible additive manufacturing cycle for generating open cell stents with diameter variations, while several points remain open. Future works will concentrate on surface finishing as well as further microstructural characterization and mechanical testing.

Acknowledgments

The authors gratefully acknowledge the technical support provided by Alberto Coda and Jannis Lemke from SAES Getters Spa. The Italian Ministry of Education, University and Research is acknowledged for the support provided through the Project “Department of Excellence LIS4.0 - Lightweight and Smart Structures for Industry 4.0”.

References

[1] J.W. Olin, B.A. Sealove, Peripheral Artery Disease: Current Insight Into the Disease and Its Diagnosis and Management, Mayo Clinic Proceedings. 85 (2010) 678–692. https://doi.org/10/fqd4jz.

[2] J.D. Santilli, S.M. Santilli, Chronic critical limb ischemia: diagnosis, treatment and prognosis, Am Fam Physician. 59 (1999) 1899–1908.

[3] K. Maleckis, E. Anttila, P. Aylward, W. Poulson, A. Desyatova, J. MacTaggart, A. Kamenskiy, Nitinol Stents in the Femoropopliteal Artery: A Mechanical Perspective on Material, Design, and Performance, Ann Biomed Eng. 46 (2018) 684–704. https://doi.org/10.1007/s10439-018-1990-1.

[4] S.M. Patel, J. Li, S.A. Parikh, Design and Comparison of Large Vessel Stents, Interventional Cardiology Clinics. 5 (2016) 365–380. https://doi.org/10.1016/j.iccl.2016.03.005.

[5] P. Björkman, E. Peltola, A. Albäck, M. Venermo, Peripheral Vascular Restenosis: A Retrospective Study on the Use of Drug-Eluting Balloons in Native Arteries, Vein Grafts and Dialysis Accesses, Scand J Surg. 106 (2017) 158–164. https://doi.org/10/ggjs66.

[6] D. Stoeckel, A. Pelton, T. Duerig, Self-expanding nitinol stents: material and design considerations, Eur Radiol. 14 (2004) 292–301. https://doi.org/10/bq8pgf.

[7] L.M. Schetky, M.H. Wu, Issues in the further development of nitinol properties and processing for medical device applications, in: Shrivastava S, Editor. Medical Device Materials: Proceedings of the Materials & Processes for Medical Devices Conference. ASM International, 2004: pp. 271–276.

[8] A.G. Demir, B. Previtali, Additive manufacturing of cardiovascular CoCr stents by selective laser melting, Materials & Design. 119 (2017) 338–350. https://doi.org/10.1016/j.matdes.2017.01.091.

[9] A.G. Demir, P. Colombo, B. Previtali, From pulsed to continuous wave emission in SLM with contemporary fiber laser sources: effect of temporal and spatial pulse overlap in part quality, Int J Adv Manuf Technol. 91 (2017) 2701–2714. https://doi.org/10/gbk26d.

[10] G. Catalano, A.G. Demir, V. Furlan, B. Previtali, Prototyping of biodegradable flat stents in pure zinc by laser microcutting and chemical etching, J. Micromech. Microeng. 28 (2018) 095016. https://doi.org/10.1088/1361-6439/aac83d.

[11] V. Finazzi, A.G. Demir, C.A. Biffi, C. Chiastra, F. Migliavacca, L. Petrini, B. Previtali, Design Rules for Producing Cardiovascular Stents by Selective Laser Melting: Geometrical Constraints and Opportunities, Procedia Structural Integrity. 15 (2019) 16–23. https://doi.org/10.1016/j.prostr.2019.07.004.

[12] V. Finazzi, A.G. Demir, C.A. Biffi, F. Migliavacca, L. Petrini, B. Previtali, Design and functional testing of a novel balloon-expandable cardiovascular stent in CoCr alloy produced by selective laser melting, Journal of Manufacturing Processes. 55 (2020) 161–173. https://doi.org/10/gg2czc.

[13] Y. Wessarges, R. Hagemann, Additive Manufacturing of Vascular Implants by Selective Laser Melting, Biomedical Engineering / Biomedizinische Technik. 59 (2014). https://doi.org/10.1515/bmt-2014-5005.

[14] P. Wen, M. Voshage, L. Jauer, Y. Chen, Y. Qin, R. Poprawe, J.H. Schleifenbaum, Laser additive manufacturing of Zn metal parts for biodegradable applications: Processing, formation quality and mechanical properties, Materials & Design. 155 (2018) 36–45. https://doi.org/10/ggm59k.

[15] K. Cooper, P. Steele, B. Cheng, K. Chou, Contact-Free Support Structures for Part Overhangs in Powder-Bed Metal Additive Manufacturing, Inventions. 3 (2018) 2. https://doi.org/10/gjgq2j.
[16] A.T. Clare, P.R. Chalker, S. Davies, C.J. Sutcliffe, S. Tsopanos, Selective laser melting of high aspect ratio 3D nickel–titanium structures two way trained for MEMS applications, Int J Mech Mater Des. 4 (2008) 181–187. https://doi.org/10.1007/s10999-007-9032-4.
[17] C.A. Biffi, A. Tuissi, A.G. Demir, Martensitic transformation, microstructure and functional behavior of thin-walled Nitinol produced by micro laser metal wire deposition, Journal of Materials Research and Technology. 12 (2021) 2205–2215. https://doi.org/10.1016/j.jmrt.2021.03.108.
[18] T.E. Abioye, P.K. Farayibi, P. Kinnel, A.T. Clare, Functionally graded Ni-Ti microstructures synthesised in process by direct laser metal deposition, Int J Adv Manuf Technol. 79 (2015) 843–850. https://doi.org/10.1007/s00170-015-6878-8.
[19] Z.X. Khoo, J.E.M. Teoh, Y. Liu, C.K. Chua, S. Yang, J. An, K.F. Leong, W.Y. Yeong, 3D printing of smart materials: A review on recent progresses in 4D printing, Virtual and Physical Prototyping. 10 (2015) 103–122. https://doi.org/10.1080/17452759.2015.1097054.
[20] T. Bormann, B. Müller, M. Schinhammer, A. Kessler, P. Thalmann, M. de Wild, Microstructure of selective laser melted nickel–titanium, Materials Characterization. 94 (2014) 189–202. https://doi.org/10.1016/j.matchar.2014.05.017.
[21] S. Dadbakhsh, M. Speirs, J. Van Humbeeck, J.-P. Kruth, Laser additive manufacturing of bulk and porous shape-memory NiTi alloys: From processes to potential biomedical applications, MRS Bull. 41 (2016) 765–774. https://doi.org/10.1557/mrs.2016.209.
[22] M. Speirs, X. Wang, S. Van Baelen, A. Ahadi, S. Dadbakhsh, J.-P. Kruth, J. Van Humbeeck, On the Transformation Behavior of NiTi Shape-Memory Alloy Produced by SLM, Shap. Mem. Superelasticity. 2 (2016) 310–316. https://doi.org/10.1007/s40830-016-0083-y.
[23] T. Bormann, R. Schumacher, B. Müller, M. Mertmann, M. de Wild, Tailoring Selective Laser Melting Process Parameters for NiTi Implants, Journal of Materials Engineering and Performance. 21 (2012) 2519–2524. https://doi.org/10.1007/s11665-012-0318-9.
[24] X. Wang, S. Kustov, J. Van Humbeeck, A Short Review on the Microstructure, Transformation Behavior and Functional Properties of NiTi Shape Memory Alloys Fabricated by Selective Laser Melting, Materials. 11 (2018) 1683. https://doi.org/10.3390/ma11091683.
[25] S. Saedi, N. Shayesteh Moghaddam, A. Amerinatanzi, M. Elahinia, H.E. Karaca, On the effects of selective laser melting process parameters on microstructure and thermomechanical response of Ni-rich NiTi, Acta Materialia. 144 (2018) 552–560. https://doi.org/10/gc223x.
[26] J. Sam, B. Franco, J. Ma, I. Karaman, A. Elwany, J.H. Mabe, Tensile actuation response of additively manufactured nickel-titanium shape memory alloys, Scripta Materialia. 146 (2018) 164–168. https://doi.org/10/gc27gf.
[27] S. Dadbakhsh, B. Vrancken, J.-P. Kruth, J. Luyten, J. Van Humbeeck, Texture and anisotropy in selective laser melting of NiTi alloy, Materials Science and Engineering: A. 650 (2016) 225–232. https://doi.org/10/f729j8.
[28] J. Frenzel, E.P. George, A. Dlouhy, Ch. Somsen, M.F.-X. Wagner, G. Eggeler, Influence of Ni on martensitic phase transformations in NiTi shape memory alloys, Acta Materialia. 58 (2010) 3444–3458. https://doi.org/10.1016/j.actamat.2010.02.019.

[29] J.M. Walker, C. Haberland, M. Taheri Andani, H.E. Karaca, D. Dean, M. Elahinia, Process development and characterization of additively manufactured nickel–titanium shape memory parts, Journal of Intelligent Material Systems and Structures. 27 (2016) 2653–2660. https://doi.org/10.1177/1045389X16635848.
[30] M. Andani, C. Haberland, J.M. Walker, M. Karamooz, A. Sadi Turabi, S. Saedi, R. Rahmanian, H. Karaca, D. Dean, M. Kadkhodaei, M. Elahinia, Achieving biocompatible stiffness in NiTi through additive manufacturing, Journal of Intelligent Material Systems and Structures. 27 (2016) 2661–2671. https://doi.org/10.1177/1045389X16641199.
[31] J. Walker, M.T. Andani, C. Haberland, M. Elahinia, Additive Manufacturing of Nitinol Shape Memory Alloys to Overcome Challenges in Conventional Nitinol Fabrication, in: Volume 2A: Advanced Manufacturing, ASME, Montreal, Quebec, Canada, 2014: p. V02AT02A037. https://doi.org/10.1115/IMECE2014-40432.
[32] Z. Khoo, J. An, C. Chua, Y. Shen, C. Kuo, Y. Liu, Effect of Heat Treatment on Repetitively Scanned SLM NiTi Shape Memory Alloy, Materials. 12 (2018) 77. https://doi.org/10.3390/ma12010077.
[33] M.R. Karamooz-Ravari, M. Taheri Andani, M. Kadkhodaei, S. Saedi, H. Karaca, M. Elahinia, Modeling the cyclic shape memory and superelasticity of selective laser melting fabricated NiTi, International Journal of Mechanical Sciences. 138–139 (2018) 54–61. https://doi.org/10.1016/j.ijmecsci.2018.01.034.
[34] S. Dadbakhsh, M. Speirs, J.-P. Kruth, J. Schrooten, J. Luyten, J. Van Humbeeck, Effect of SLM Parameters on Transformation Temperatures of Shape Memory Nickel Titanium Parts: Effect of SLM Parameters on Transformation Temperatures of NiTi, Adv. Eng. Mater. 16 (2014) 1140–1146. https://doi.org/10.1002/adem.201300558.
[35] Z.X. Khoo, Y. Liu, Z.H. Low, J. An, C.K. Chua, K.F. Leong, Fabrication of SLM NiTi Shape Memory Alloy via Repetitive Laser Scanning, Shape Memory and Superelasticity. 4 (2018) 112–120. https://doi.org/10.1007/s40830-017-0139-7.
[36] S.-F. Ou, B.-Y. Peng, Y.-C. Chen, M.-H. Tsai, Manufacturing and Characterization of NiTi Alloy with Functional Properties by Selective Laser Melting, Metals. 8 (2018) 342. https://doi.org/10.3390/met8050342.
[37] M. Taheri Andani, S. Saedi, A.S. Turabi, M.R. Karamooz, C. Haberland, H.E. Karaca, M. Elahinia, Mechanical and shape memory properties of porous Ni 50.1 Ti 49.9 alloys manufactured by selective laser melting, Journal of the Mechanical Behavior of Biomedical Materials. 68 (2017) 224–231. https://doi.org/10.1016/j.jmbbm.2017.01.047.
[38] R.F. Hamilton, B.A. Bimber, M. Taheri Andani, M. Elahinia, Multi-scale shape memory effect recovery in NiTi alloys additive manufactured by selective laser melting and laser directed energy deposition, Journal of Materials Processing Technology. 250 (2017) 55–64. https://doi.org/10.1016/j.jmatprotec.2017.06.027.
[39] C. Haberland, M. Elahinia, J.M. Walker, H. Meier, J. Frenzel, On the development of high quality NiTi shape memory and pseudoelastic parts by additive manufacturing, Smart Materials and Structures. 23 (2014) 104002. https://doi.org/10.1088/0964-1726/23/10/104002.
[40] H. Meier, C. Haberland, J. Frenzel, Structural and functional properties of NiTi shape memory alloys produced by Selective Laser Melting, in: 2012. https://doi.org/10.1201/b11341-47.

[41] S. Saedi, A.S. Turabi, M.T. Andani, N.S. Moghaddam, M. Elahinia, H.E. Karaca, Texture, aging, and superelasticity of selective laser melting fabricated Ni-rich NiTi alloys, Materials Science and Engineering: A. 686 (2017) 1–10. https://doi.org/10.1016/j.msea.2017.01.008.
[42] C. Zhao, H. Liang, S. Luo, J. Yang, Z. Wang, The effect of energy input on reaction, phase transition and shape memory effect of NiTi alloy by selective laser melting, J. Alloy. Compd. 817 (2020) 153288. https://doi.org/10/ggj3x5.
[43] M. Elahinia, N. Shayesteh Moghaddam, M. Taheri Andani, A. Amerinatanzi, B.A. Bimber, R.F. Hamilton, Fabrication of NiTi through additive manufacturing: A review, Progress in Materials Science. 83 (2016) 630–663. https://doi.org/10.1016/j.pmatsci.2016.08.001.
[44] Z. Xiong, Z. Li, Z. Sun, S. Hao, Y. Yang, M. Li, C. Song, P. Qiu, L. Cui, Selective laser melting of NiTi alloy with superior tensile property and shape memory effect, Journal of Materials Science & Technology. 35 (2019) 2238–2242. https://doi.org/10.1016/j.jmst.2019.05.015.
[45] Q. Zhang, S. Hao, Y. Liu, Z. Xiong, W. Guo, Y. Yang, Y. Ren, L. Cui, L. Ren, Z. Zhang, The microstructure of a selective laser melting (SLM)-fabricated NiTi shape memory alloy with superior tensile property and shape memory recoverability, Applied Materials Today. 19 (2020) 100547. https://doi.org/10/ggnjrd.
[46] N. Shayesteh Moghaddam, S. Saedi, A. Amerinatanzi, A. Hinojos, A. Ramazani, J. Kundin, M.J. Mills, H. Karaca, M. Elahinia, Achieving superelasticity in additively manufactured NiTi in compression without post-process heat treatment, Sci Rep. 9 (2019) 41. https://doi.org/10.1038/s41598-018-36641-4.
[47] X. Wang, M. Speirs, S. Kustov, B. Vrancken, X. Li, J.-P. Kruth, J. Van Humbeeck, Selective laser melting produced layer-structured NiTi shape memory alloys with high damping properties and Elinvar effect, Scripta Materialia. 146 (2018) 246–250. https://doi.org/10.1016/j.scriptamat.2017.11.047.
[48] S. Saedi, A.S. Turabi, M. Taheri Andani, C. Haberland, H. Karaca, M. Elahinia, The influence of heat treatment on the thermomechanical response of Ni-rich NiTi alloys manufactured by selective laser melting, Journal of Alloys and Compounds. 677 (2016) 204–210. https://doi.org/10.1016/j.jallcom.2016.03.161.
[49] L. Caprio, A.G. Demir, B. Previtali, Comparative study between CW and PW emissions in selective laser melting, Journal of Laser Applications. 30 (2018) 032305. https://doi.org/10.2351/1.5040631.
[50] C.A. Biffi, P. Bassani, J. Fiocchi, A. Tuissi, Microstructural and Mechanical Response of NiTi Lattice 3D Structure Produced by Selective Laser Melting, Metals. 10 (2020) 814. https://doi.org/10.3390/met10060814.
[51] A. Nespoli, P. Bettini, E. Villa, G. Sala, F. Passaretti, A.M. Grande, A Study on Damping Property of NiTi Elements Produced by Selective Laser-Beam Melting, Advanced Engineering Materials. 23 (2021) 2001246. https://doi.org/10.1002/adem.202001246.
[52] A. Nespoli, A.M. Grande, N. Bennato, D. Rigamonti, P. Bettini, E. Villa, G. Sala, F. Passaretti, Towards an understanding of the functional properties of NiTi produced by powder bed fusion, Prog Addit Manuf. 6 (2021) 321–337. https://doi.org/10.1007/s40964-020-00155-1.
[53] D. Carluccio, A.G. Demir, L. Caprio, B. Previtali, M.J. Bermingham, M.S. Dargusch, The influence of laser processing parameters on the densification and surface morphology of pure Fe and Fe-

35Mn scaffolds produced by selective laser melting, Journal of Manufacturing Processes. 40 (2019) 113–121. https://doi.org/10.1016/j.jmapro.2019.03.018.
[54] X. Huang, Y. Liu, Effect of annealing on the transformation behavior and superelasticity of NiTi shape memory alloy, Scripta Materialia. 45 (2001) 153–160. https://doi.org/10.1016/S1359-6462(01)01005-3.
[55] B. Brown, J. Newkirk, F. Liou, Absorption of Nitrogen during Pulsed Wave L-PBF of 17-4 PH Steel, Materials (Basel). 14 (2021). https://doi.org/10/gjgv2p.
[56] A.G. Demir, B. Previtali, N. Lecis, Development of laser dimpling strategies on TiN coatings for tribological applications with a highly energetic Q-switched fibre laser, Optics & Laser Technology. 54 (2013) 53–61. https://doi.org/10.1016/j.optlastec.2013.05.007.
[57] C. Velmurugan, V. Senthilkumar, S. Dinesh, D. Arulkirubakaran, Review on phase transformation behavior of NiTi shape memory alloys, Materials Today: Proceedings. 5 (2018) 14597–14606. https://doi.org/10.1016/j.matpr.2018.03.051.
[58] T.W. Duerig, A.R. Pelton, K. Bhattacharya, The Measurement and Interpretation of Transformation Temperatures in Nitinol, Shap. Mem. Superelasticity. 3 (2017) 485–498. https://doi.org/10/gf824r.
[59] F. Khaleghi, J. Khalil-Allafi, V. Abbasi-Chianeh, S. Noori, Effect of short-time annealing treatment on the superelastic behavior of cold drawn Ni-rich NiTi shape memory wires, Journal of Alloys and Compounds. 554 (2013) 32–38. https://doi.org/10.1016/j.jallcom.2012.11.183.
[60] F. Cardarelli, Materials handbook: a concise desktop reference, 2. ed, Springer, London, 2008.
[61] X. Wang, J. Yu, J. Liu, L. Chen, Q. Yang, H. Wei, J. Sun, Z. Wang, Z. Zhang, G. Zhao, J. Van Humbeeck, Effect of process parameters on the phase transformation behavior and tensile properties of NiTi shape memory alloys fabricated by selective laser melting, Additive Manufacturing. 36 (2020) 101545. https://doi.org/10/gjk3p4.